

IRS-Aided Radar: Enhanced Target Parameter Estimation via Intelligent Reflecting Surfaces

Zahra Esmaeilbeig^{†,1}, Kumar Vijay Mishra^{†,2}, and Mojtaba Soltanalian^{†,3}

[†] Department of Electrical and Computer Engineering

University of Illinois at Chicago, Chicago, Illinois, USA

[‡]United States DEVCOM Army Research Laboratory, Adelphi, Maryland, USA

Email: {¹zesmae2, ³msol}@uic.edu, ²kvm@ieee.org

Abstract—The intelligent reflecting surface (IRS) technology has recently attracted a lot of interest in wireless communications research. An IRS consists of passive reflective elements capable of tuning the phase, amplitude, frequency, and polarization of impinging waveforms. We investigate the deployment of IRS to aid radar systems when the line-of-sight (LoS) link to the targets is weak or blocked. We demonstrate that deployment of multiple IRS platforms provides a virtual or non-line-of-sight (NLoS) link between the radar and target leading to an enhanced radar performance. Numerical experiments indicate that the IRS enhances the target parameter estimation when the LoS link is weaker by $\sim 10^{-1}$ in comparison to the NLoS link.

Index Terms—Intelligent reflecting surface, radar, programmable metasurfaces, target estimation, wireless communications, Cramér-Rao bound.

I. INTRODUCTION

An intelligent reflecting surface (IRS) is composed of a large number of passive reconfigurable meta-material elements, which reflect the incoming signal by introducing a predetermined phase shift [1]. In a communication system, this phase shift is controlled via an external signal transmitted by the base station (BS) through a backhaul control link. As a result, the incoming signal from the BS is manipulated in real time, thereby, efficiently reflecting the received signal toward the users [2–5]. The IRS technology has appeared in wireless communications, also under other names including large intelligent surface and software-controlled metasurfaces [6–8]. Several promising IRS use-cases including range extension to users with obstructed direct links [6], physical layer security [9], and unmanned air vehicle (UAV) communications [10] have been studied. Some prior works on IRS-assisted signal transmission are [10–14].

In this context, IRS deployment has an untapped potential in radar system design and signal processing for target detection and estimation [15]–[16]. In an IRS-aided radar, the surface manipulates the signal coming from the radar transmitter (target) and reflects it toward the target (radar receiver) (Fig. 1). Lately, IRS has emerged as a promising and cost-effective solution to establish robust connections even when the line-of-sight (LoS) link is blocked by obstructions [17]. There have been several prior works on non-line-of-sight (NLoS) radar

systems without the aid of IRS [18–20]. However, these techniques require knowledge of the entire geometric structure of the environment. In addition, processing the multipath returns from a target is computationally demanding. The IRS-aided NLoS radar is a paradigm shift because the location of the IRS platforms and flexibility in beamforming via IRS are sufficient to perform target detection and estimation. By smartly tuning the phase shifts of IRS passive elements, effective NLoS or virtual LoS links are created thereby yielding a more reliable sensing of targets.

The IRS-aided radar for NLoS scenarios was introduced in [21] and extended to multiple-input multiple-output (MIMO) radar in [22, 23]. In this paper, we develop a mathematical model for IRS-aided radar parameter estimation and investigate the potential gains associated with the IRS deployment in such settings. Contrary to most prior works [21–23] that focused on the NLoS sensing via a single IRS, we incorporate multiple IRS platforms [24–26]. We develop the general signal model for a multiple IRS-aided radar, in which the IRS acts as a phase shift component and benchmark the performance of IRS platforms through mean square error of target parameter estimation. We derive the best linear unbiased estimator (BLUE) for estimating the target back-scattering coefficient. Our numerical experiments show that using IRS even with randomly chosen phase shifts improve the mean-squared-error of target parameter estimation. We further study the optimization of the IRS platform by designing phase shifts to specifically minimize the mean-squared-error of target parameter estimation. As expected, the optimized IRS case leads to lower estimation error in comparison with the non-optimized IRS. We further derive the Cramér-Rao bound (CRB) for estimation of the target parameter and illustrate it for the LoS and NLoS scenarios.

Throughout this paper, we use bold lowercase letters for vectors and bold uppercase letters for matrices. The notations $(\cdot)^T$ and $(\cdot)^H$ denote the vector/matrix transpose and the Hermitian transpose, respectively. The symbols \odot and \otimes stand for the Hadamard (element-wise) and Kronecker product of matrices; $\text{Tr}(\cdot)$ is the trace operator for matrices; $\text{Diag}(\cdot)$ denotes the diagonalization operator that produces a diagonal matrix with same diagonal entries as the entries of its vector argument; and $\text{diag}(\cdot)$ outputs a vector containing the diagonal entries of the input matrix. $\|\cdot\|_2$ is the ℓ_2 norm. Finally, $\arg(\cdot)$,

This work was supported in part by the U.S. National Science Foundation Grant ECCS-1809225.

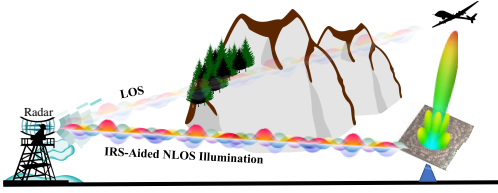


Fig. 1. An illustration of IRS-aided radar operation. The IRS creates effective virtual LoS links between the radar and the desired targets. Large IRS platforms may be required for far-field deployment.

$\text{Re}(\cdot)$ and $\text{Im}(\cdot)$ return the arguments, real part and imaginary part of a complex input vector, respectively.

II. SYSTEM MODEL

Consider a pulse-Doppler radar system that transmits a train of N uniformly-spaced pulses $x(t)$, each of which is nonzero over the support $[0, T_p]$, as

$$s(t) = \sum_{n=0}^{N-1} x(t - nT_{\text{PRI}}), \quad 0 \leq t \leq (N-1)T_{\text{PRI}}, \quad (1)$$

where T_{PRI} is the pulse repetition interval (PRI). The entire duration of all N pulses is the coherent processing interval (CPI) (“slow time”). Assume the target scene consists of a single Swerling-0 model [27] moving target, characterized by unknown parameters: complex reflectivity/amplitude α_T and the normalized target Doppler shift ν (expressed in radians) relative to the radar; note that, in the formulation of this paper, the target range is assumed to be known.

In the absence of an IRS, the transmit signal is reflected back from the target and collected by the radar receiver (Fig. 2). The baseband continuous-time received signal is

$$\begin{aligned} y(t) &= \alpha_T h_{\text{LoS}} \sum_{n=0}^{N-1} x(t - nT_{\text{PRI}}) e^{j\nu t} + n(t), \\ &\approx \alpha_T h_{\text{LoS}} \sum_{n=0}^{N-1} x(t - nT_{\text{PRI}}) e^{j\nu n T_p} + n(t), \end{aligned} \quad (2)$$

where $n(t)$ is random additive noise, h_{LoS} accounts for the radar-target-radar channel state information (CSI), and the last approximation follows from the fact that $\nu \ll 1/T_p$ so that the phase rotation within the CPI could be approximated as a constant.

Each snapshot of the received signal are sampled at the rate $1/T_p$ yielding a total of $\lfloor T_{\text{PRI}}/T_p \rfloor$ “fast-time” samples. As mentioned earlier, we assume the range of the target is known. At this fixed target range in fast-time, we collect all N slow-time samples of the received signal corresponding to each pulse in the vector $\mathbf{y} = [y(0), y(T_p), \dots, y((N-1)T_p)]^T$ as

$$\mathbf{y} = \alpha_T h_{\text{LoS}} [\mathbf{x} \odot \mathbf{p}(\nu)] + \mathbf{n}, \quad (3)$$

where $\mathbf{p}(\nu) = [1, e^{jT_p\nu}, \dots, e^{j(N-1)T_p\nu}]^T$, $\mathbf{x} = [\mathbf{x}(0), \mathbf{x}(T_p), \dots, \mathbf{x}((N-1)T_p)]^T$ and $\mathbf{n} = [n(0), n(T_p), \dots, n((N-1)T_p)]^T$ are, respectively, transmit and noise signal vectors and \mathbf{n} is zero-mean random vector with covariance matrix \mathbf{R} [28].

We now consider the received signal in the presence of an IRS (Fig. 3). Assume K IRS platforms are deployed and NLoS paths are realized through IRS platforms between the radar and target. An IRS is typically deployed as an array of discrete scattering elements. Each element (also known as a meta-atom or lattice) has the ability to introduce a phase shift to an incident wave. Assume that each IRS is equipped with M reflecting elements. Each IRS element reflects the incident signal with a phase shift and amplitude change that is configured via a smart controller. Define

$$\Theta_k = \text{Diag}(\beta_{k,1} e^{j\theta_{k,1}}, \dots, \beta_{k,M} e^{j\theta_{k,M}}) \quad (4)$$

as the phase-shift matrix of the k -th IRS, where $\theta_{k,m} \in [0, 2\pi]$, and $\beta_{k,m} \in [0, 1]$ are, respectively, phase shift and amplitude reflection gain associated with the m -th passive element of the k -th IRS. In general, it suffices to design only the phase-shift so that $\beta_{k,m} = 1$ for all (k, m) [24, 29–31].

The path via the k -th IRS is characterized by the corresponding CSI $h_{\text{NLoS},k}$, IRS phase shift matrix Θ_k , Doppler shift ν_k , and the target reflectivity amplitude $\alpha_{T,k}$. Denote the radar-IRS $_k$ and target-IRS $_k$ CSI by, respectively, $\mathbf{g}_k \in \mathbb{C}^M$ and $\mathbf{h}_k \in \mathbb{C}^M$. The CSI for all the paths between radar, target and IRS platforms are assumed to be well-estimated through suitable channel estimation techniques [32]. We define $\mathbf{h}_{\text{NLoS}} = [h_{\text{NLoS},k}, \dots, h_{\text{NLoS},K}]^T$ as the NLoS CSI vector. Using the channel reciprocity of IRS [33], the NLoS CSI is

$$\mathbf{h}_{\text{NLoS}} = \left[|\mathbf{h}_1^H \Theta_1 \mathbf{g}_1|^2, \dots, |\mathbf{h}_K^H \Theta_K \mathbf{g}_K|^2 \right]^T. \quad (5)$$

The received signal is a superposition of the reflected signals from all NLoS paths as

$$\mathbf{y} = \alpha_T h_{\text{LoS}} [\mathbf{x} \odot \mathbf{p}(\nu)] + \sum_{k=1}^K \alpha_{T,k} h_{\text{NLoS},k} [\mathbf{x} \odot \mathbf{p}(\nu_k)] + \mathbf{n}. \quad (6)$$

While both LoS and NLoS signals are available at the receiver, we aim to show the effectiveness of IRS-created NLoS in overcoming obstructed or weak LoS links. Therefore, throughout this paper, we consider the case when the LoS link strength is insignificant, i.e. $h_{\text{LoS}} \simeq \mathbf{0}$ and the signal received through NLoS is used to obtain target information. Denote the complex reflectivity vector by $\boldsymbol{\alpha} = [\alpha_{T,1}, \alpha_{T,2}, \dots, \alpha_{T,K}]^T$ of a moving target for $k \in \{1, \dots, K\}$ paths. Rewrite the received signal in (6) compactly as

$$\mathbf{y} = \mathbf{A}\boldsymbol{\alpha} + \mathbf{n}, \quad (7)$$

where $\mathbf{A} = [\mathbf{a}_1, \dots, \mathbf{a}_K] \in \mathbb{C}^{N \times K}$ is the sensing matrix with columns

$$\mathbf{a}_k \triangleq \mathbf{h}_{\text{NLoS},k} [\mathbf{x} \odot \mathbf{p}(\nu_k)]. \quad (8)$$

Our goal is to obtain BLUE for $\alpha_{T,k}$ for all k paths.

III. IRS-AIDED TARGET PARAMETER ESTIMATION

Following the Gauss-Markov theorem [36], the BLUE for $\boldsymbol{\alpha}$ is

$$\hat{\boldsymbol{\alpha}} = (\mathbf{A}^H \mathbf{R}^{-1} \mathbf{A})^{-1} \mathbf{A}^H \mathbf{R}^{-1} \mathbf{y}. \quad (9)$$



Fig. 2. LoS link between the radar and the target

The covariance matrix of $\hat{\alpha}$ is

$$\mathbf{C}_{\hat{\alpha}} = (\mathbf{A}^H \mathbf{R}^{-1} \mathbf{A})^{-1}, \quad (10)$$

with the minimum achieved variance for $\hat{\alpha}_k$ given by $\text{var}(\hat{\alpha}_k) = \left[(\mathbf{A}^H \mathbf{R}^{-1} \mathbf{A})^{-1} \right]_{kk}$. The overall mean-squared-error (MSE) of the proposed estimator is thus $\text{MSE}(\hat{\alpha}) = \text{Tr} \left((\mathbf{A}^H \mathbf{R}^{-1} \mathbf{A})^{-1} \right)$. The optimal phase-shift matrices $\{\Theta_k\}$, $k \in \{1, \dots, K\}$ to minimize the MSE of target cross-section parameter are obtained by solving the following problem

$$\underset{\Theta_k, k \in \{1, \dots, K\}}{\text{minimize}} \text{MSE}(\hat{\alpha}) = \underset{\Theta_k, k \in \{1, \dots, K\}}{\text{minimize}} \text{Tr} \left((\mathbf{A}^H \mathbf{R}^{-1} \mathbf{A})^{-1} \right). \quad (11)$$

The following theorem states that the optimal phase shifts of the K different IRS platforms are decoupled. Also, the optimal phase shift for IRS $_k$ compensates for the total phases in the channels \mathbf{g}_k and \mathbf{h}_k .

Theorem 1. *The solution to the optimization problem*

$$\underset{\Theta_k, k \in \{1, \dots, K\}}{\text{minimize}} \text{MSE}(\hat{\alpha}), \quad (12)$$

is

$$\Theta_k^* = \text{Diag} \left(e^{j \arg(\mathbf{c}_k)} \right), \quad (13)$$

where $\mathbf{c}_k \triangleq \text{Diag}(\mathbf{g}_k)^H \mathbf{h}_k$.

Proof. Define the IRS-observed Doppler shift matrix as $\mathbf{P}(\nu) \triangleq [\mathbf{p}(\nu_1), \dots, \mathbf{p}(\nu_K)] \in \mathbb{C}^{N \times K}$. Incorporating this definition in (7)-(8), we have $\mathbf{A} = \text{Diag}(\mathbf{x}) \mathbf{P}(\nu) \text{Diag}(\mathbf{h}_{\text{NLoS}})$, which is used to compute

$$(\mathbf{A}^H \mathbf{R}^{-1} \mathbf{A})^{-1} = \mathbf{A}^{-1} \mathbf{R} \mathbf{A}^{-H} = \text{Diag}(\mathbf{h}_{\text{NLoS}})^{-1} \Psi \text{Diag}(\mathbf{h}_{\text{NLoS}})^{-H}, \quad (14)$$

with $\Psi \triangleq \Omega^{-1} \mathbf{R} \Omega^H$ and $\Omega \triangleq \text{Diag}(\mathbf{x}) \mathbf{P}(\nu)$. Substituting (14) in (11) yields the optimization problem

$$\underset{\Theta_k, k \in \{1, \dots, K\}}{\text{minimize}} \sum_{k=1}^K |h_{\text{NLoS},k}|^{-2} \Psi_{kk} = \underset{\Theta_k, k \in \{1, \dots, K\}}{\text{maximize}} \left| \mathbf{h}_k^H \Theta_k \mathbf{g}_k \right|.$$

Considering the property $\mathbf{a} \odot \mathbf{b} = \text{Diag}(\mathbf{a}) \mathbf{b}$ of the Hadamard product as well as the diagonal structure of Θ_k , we write

$$\mathbf{h}_k^H \Theta_k \mathbf{g}_k = \mathbf{h}_k^H [\text{diag}(\Theta_k) \odot \mathbf{g}_k] = \mathbf{c}_k^H \text{diag}(\Theta_k). \quad (15)$$

It now follows that the optimal solution to (11) is (13). \square

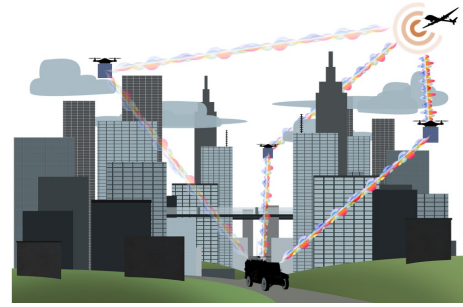


Fig. 3. NLoS or virtual LoS link between the radar and the target provided by $K = 3$ IRS platforms.

IV. ERROR BOUND ANALYSIS

We analyze the CRB of the proposed IRS-aided target parameter estimation. Assume

$$\tilde{\alpha} = [\alpha_R^T, \alpha_I^T]^T \quad (16)$$

with $\alpha_R = \text{Re}(\alpha)$, $\alpha_I = \text{Im}(\alpha)$. For an unbiased estimator of the parameter α , the covariance matrix of $\hat{\alpha}$ is lower bounded as $\mathbf{C}_{\hat{\alpha}} = \mathbf{E}\{(\hat{\alpha} - \tilde{\alpha})(\hat{\alpha} - \tilde{\alpha})^H\} \geq \mathbf{C}_{\text{CRB}}$, in the sense that the difference $\mathbf{C}_{\hat{\alpha}} - \mathbf{C}_{\text{CRB}}$ is a positive semidefinite matrix [36–39]. We divide the Fisher information matrix (FIM), \mathbf{J} into submatrices as

$$\mathbf{J} = \begin{bmatrix} \mathbf{J}_{\alpha_R, \alpha_R} & \mathbf{J}_{\alpha_R, \alpha_I} \\ \mathbf{J}_{\alpha_I, \alpha_R} & \mathbf{J}_{\alpha_I, \alpha_I} \end{bmatrix}. \quad (17)$$

Using the Slepian-Bangs formula [40] for the observation vector \mathbf{y} , with a Gaussian distribution $\mathbf{y} \sim N(\mu, \mathbf{R})$, the (m, n) -th element of the Fisher information matrix (FIM) is

$$\mathbf{J}_{mn} = \text{Tr} \left(\mathbf{R}^{-1} \frac{\partial \mathbf{R}}{\partial \tilde{\alpha}_m} \mathbf{R}^{-1} \frac{\partial \mathbf{R}}{\partial \tilde{\alpha}_n} \right) + 2 \text{Re} \left(\frac{\partial \mu}{\partial \tilde{\alpha}_m}^H \mathbf{R}^{-1} \frac{\partial \mu}{\partial \tilde{\alpha}_n} \right). \quad (18)$$

Following (7), we have $\mu = \mathbf{A} \alpha$. The FIM elements are

$$\begin{aligned} [\mathbf{J}_{\alpha_R, \alpha_R}]_{mn} &= 2 \text{Re} \left(\frac{\partial \mu}{\partial \alpha_{R_m}}^H \mathbf{R}^{-1} \frac{\partial \mu}{\partial \alpha_{R_n}} \right) = 2 \text{Re} \left(\mathbf{a}_m^H \mathbf{R}^{-1} \mathbf{a}_n \right) \\ &= 2 \text{Re} \left(\mathbf{a}_m^H \mathbf{R}^{-1} \mathbf{a}_m \right) = 2 \text{Re} \left(\mathbf{e}_m^T \mathbf{A}^H \mathbf{R}^{-1} \mathbf{A} \mathbf{e}_m \right), \end{aligned} \quad (19)$$

where \mathbf{e}_m is a $K \times 1$ vector, whose m -th element is unity and remaining elements are zero. Similarly, other submatrices of the FIM are

$$\begin{aligned} \mathbf{J}_{\alpha_I, \alpha_I} &= \mathbf{J}_{\alpha_R, \alpha_R} = 2 \text{Re} \left(\mathbf{A}^H \mathbf{R}^{-1} \mathbf{A} \right), \\ \mathbf{J}_{\alpha_R, \alpha_I} &= -\mathbf{J}_{\alpha_I, \alpha_R} = -2 \text{Im} \left(\mathbf{A}^H \mathbf{R}^{-1} \mathbf{A} \right). \end{aligned} \quad (20)$$

substituting (20) in (17), we get

$$\mathbf{J} = 2 \text{Re} \left([1 \ j]^H \otimes [1 \ j] \otimes (\mathbf{A}^H \mathbf{R}^{-1} \mathbf{A}) \right), \quad (21)$$

the inverse of which yields $\mathbf{C}_{\text{CRB}} = \mathbf{J}^{-1}$.

V. NUMERICAL EXPERIMENTS

We validated the performance of target parameter estimation in IRS-aided radar through numerical experiments. Throughout our experiments, $\mathbf{x} \in \mathbb{C}^N$ is a unimodular code that is randomly chosen with the length $N = 50$ i.e., $\mathbf{x}_n = e^{j\phi_n}$, $n \in \{1, \dots, 50\}$ [41]. We set $K = 5$ and $M = 10$.

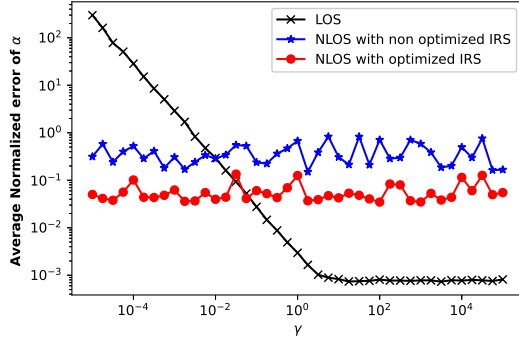


Fig. 4. NMSE for estimation of target scattering coefficient α for different values of $\gamma \in [10^{-5}, 10^5]$, $K = 5$ IRS platforms, and $M = 10$.

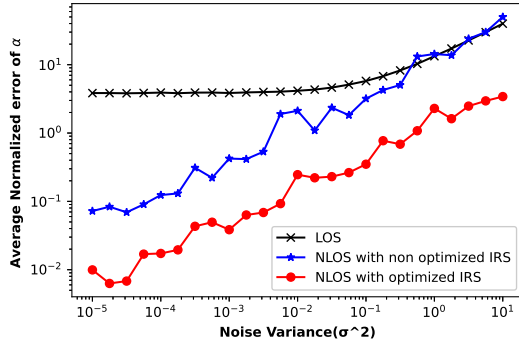


Fig. 5. Average NMSE of the recovered target scattering coefficient α for different noise variances $\sigma_n^2 \in [10^{-5}, 1]$, with $K = 5$ IRS platforms, $M = 10$ reflecting elements and the LoS-to-NLoS SNR $\gamma = 10^{-2}$.

We generated the noise vector \mathbf{n} from an independent and identically distributed random Gaussian process i.e. $\mathbf{R} = \sigma_n^2 \mathbf{I}$. We consider the following scenarios:

- An LoS path (Fig. 2) is present between the radar and target with the CSI \mathbf{h}_{LoS} .
- There is an NLoS path (Fig. 3) through K IRS platforms with non optimal $\theta_{k,m}$, $k \in \{1, \dots, K\}$ and $m \in \{1, \dots, M\}$ chosen randomly in the interval $[0, 2\pi)$.
- There is an NLoS path with the CSI \mathbf{h}_{NLoS} . The IRS phase-shift parameters Θ_k , $k \in \{1, \dots, K\}$ are optimized and set according to (13).

We define the *LoS-to-NLoS signal-to-noise ratio (SNR)* as

$$\gamma \triangleq \frac{|\alpha_T h_{\text{LoS}}|^2}{\|\alpha^T \mathbf{h}_{\text{NLoS}}\|_2^2}, \quad (22)$$

which governs the relative strengths of the LoS and NLoS links. We use the normalized estimation error of the back-scattering coefficient α , defined by $\text{NMSE} \triangleq \frac{\|\alpha - \hat{\alpha}\|_2}{\|\alpha\|_2}$, as a measure of performance for our estimators. In Fig. 4, we illustrate the effectiveness of the optimized and non-optimized IRS over different strengths of the link between the radar and the target. In order to control the LoS-to-NLoS SNR γ , we generated the LoS and NLoS channels such that $|\alpha_T h_{\text{LoS}}|^2 = \gamma$ and $\|\alpha^T \mathbf{h}_{\text{NLoS}}\|_2^2 = 1$. The CSI for all channels

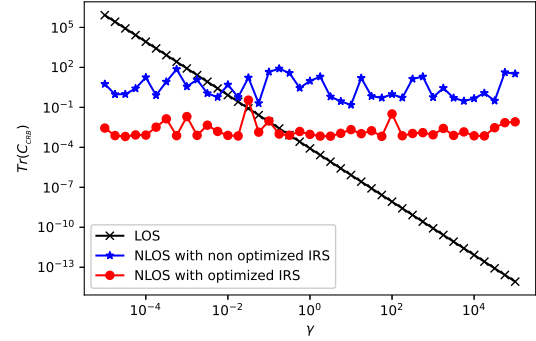


Fig. 6. The CRB of the target scattering coefficient $\tilde{\alpha}$ for different values of $\gamma \in [10^{-5}, 10^5]$, with $K = 5$ and $M = 10$.

involved is sampled from an independent circularly symmetric complex Gaussian random vector with zero mean and variance of unity and scaled such that we have $\gamma \in [10^{-5}, 10^5]$ [24]. The Doppler shifts in both the LoS and NLoS is chosen from a random uniform distribution on $[-0.5, 0.5]$ [42]. The results are averaged over 10^3 Monte-Carlo trials. The perturbations in Figs.4-6 arise from the randomness of the channels and Doppler shifts in each Monte-Carlo sample.

Fig. 4 indicates that the IRS overcomes the LoS links as weak as 10^{-1} times the NLoS link. As expected, the optimization of the IRS platform leads to lower NMSE values in comparison with the non-optimized IRS under the same LoS-to-NLoS SNR. This reveals both the potential of using the virtual link provided by IRS in place of the LoS link when it is weak or obstructed and the gains provided by IRS optimization. Fig. 5 shows the normalized estimation error of the back-scattering coefficient α with respect to the noise variance. It follows from Fig. 5 that when the LoS-to-NLoS SNR is set to 10^{-2} , the NLoS outperforms the LoS link. Fig. 6 illustrates that the CRB of the estimator $\hat{\alpha}$ in IRS-aided radar overcomes the LoS links as weak as 10^{-1} , i.e. in the same regime of γ , where IRS was effective as per the NMSE measure in Fig. 4. For illustration, the A -optimality criteria i.e. $\text{Tr}(\mathbf{C}_{\text{CRB}})$ is chosen as a scalar measure of the CRB [43].

VI. SUMMARY

We studied the deployment of IRS in narrowband radar sensing and we presented an initial study on the effectiveness of IRS in assisting target estimation in radar. The formulation proposed in this paper is useful as a baseline for other IRS-aided radar settings. We derived the optimal IRS phases in terms of the mean square error of target parameter estimation. We indicated that IRS aids in target parameter estimation when the LoS link is weaker in relative SNR by $\sim 10^{-1}$ than the NLoS link. Our numerical experiments reveal the effectiveness of the IRS even with non-optimized phase shifts.

REFERENCES

- [1] J. A. Hodge, K. V. Mishra, and A. I. Zaghoul, "Intelligent time-varying metasurface transceiver for index modulation in 6G wireless networks,"

- IEEE Antennas and Wireless Propagation Letters*, vol. 19, no. 11, pp. 1891–1895, 2020.
- [2] Ö. Özdoğan, E. Björnson, and E. G. Larsson, “Using intelligent reflecting surfaces for rank improvement in MIMO communications,” in *IEEE International Conference on Acoustics, Speech and Signal Processing*, 2020, pp. 9160–9164.
 - [3] V. S. Asadchy, M. Albooyeh, S. N. Tcvetkova, A. Díaz-Rubio, Y. Ra’di, and S. Tretyakov, “Perfect control of reflection and refraction using spatially dispersive metasurfaces,” *Physical Review B*, vol. 94, no. 7, p. 075142, 2016.
 - [4] N. M. Estakhri and A. Alu, “Wave-front transformation with gradient metasurfaces,” *Physical Review X*, vol. 6, no. 4, p. 041008, 2016.
 - [5] A. M. Elbir and K. V. Mishra, “A survey of deep learning architectures for intelligent reflecting surfaces,” *arXiv preprint arXiv:2009.02540*, 2020.
 - [6] Q. Nadeem, A. Kammoun, A. Chaaban, M. Debbah, and M. Alouini, “Large intelligent surface assisted MIMO communications,” *arXiv preprint arXiv:1903.08127*, 2019.
 - [7] E. Björnson, L. Sanguinetti, H. Wymeersch, J. Hoydis, and T. L. Marzetta, “Massive MIMO is a reality - What is next?: Five promising research directions for antenna arrays,” *Digital Signal Processing*, vol. 94, pp. 3–20, 2019.
 - [8] C. Liaskos, S. Nie, A. Tsiolaridou, A. Pitsillides, S. Ioannidis, and I. Akyildiz, “A new wireless communication paradigm through software-controlled metasurfaces,” *IEEE Communications Magazine*, vol. 56, no. 9, pp. 162–169, 2018.
 - [9] X. Guan, Q. Wu, and R. Zhang, “Intelligent reflecting surface assisted secrecy communication: Is artificial noise helpful or not?” *IEEE Wireless Communications Letters*, vol. 9, no. 6, pp. 778–782, 2020.
 - [10] S. Li, B. Duo, X. Yuan, Y.-C. Liang, and M. Di Renzo, “Reconfigurable intelligent surface assisted UAV communication: Joint trajectory design and passive beamforming,” *IEEE Wireless Communications Letters*, vol. 9, no. 5, pp. 716–720, 2020.
 - [11] Q. Wu and R. Zhang, “Intelligent reflecting surface enhanced wireless network via joint active and passive beamforming,” *IEEE Transactions on Wireless Communications*, vol. 18, no. 11, pp. 5394–5409, 2019.
 - [12] P. Wang, J. Fang, and H. Li, “Joint beamforming for intelligent reflecting surface-assisted millimeter wave communications,” *arXiv preprint arXiv:1910.08541*, 2019.
 - [13] C. Huang, A. Zappone, M. Debbah, and C. Yuen, “Achievable rate maximization by passive intelligent mirrors,” in *IEEE International Conference on Acoustics, Speech and Signal Processing*, 2018, pp. 3714–3718.
 - [14] Q. Wu and R. Zhang, “Intelligent reflecting surface enhanced wireless network: Joint active and passive beamforming design,” in *IEEE Global Communications Conference*, 2018, pp. 1–6.
 - [15] S. Khobahi, A. Bose, and M. Soltanalian, “Deep radar waveform design for efficient automotive radar sensing,” in *IEEE Sensor Array and Multichannel Signal Processing Workshop*, 2020, pp. 1–5.
 - [16] A. Bose, S. Khobahi, and M. Soltanalian, “Efficient waveform covariance matrix design and antenna selection for MIMO radar,” *Signal Processing*, vol. 183, p. 107985, 2021.
 - [17] X. Tan, Z. Sun, D. Koutsonikolas, and J. M. Jornet, “Enabling indoor mobile millimeter-wave networks based on smart reflect-arrays,” in *IEEE Conference on Computer Communications*, 2018, pp. 270–278.
 - [18] B. Watson and J. R. Guerci, *Non-line-of-sight radar*. Artech House, 2019.
 - [19] S. Guo, Q. Zhao, G. Cui, S. Li, L. Kong, and X. Yang, “Behind corner targets location using small aperture millimeter wave radar in NLOS urban environment,” *IEEE Journal of Selected Topics in Applied Earth Observations and Remote Sensing*, vol. 13, pp. 460–470, 2020.
 - [20] D. Solomitckii, M. Heino, S. Buddappagari, M. A. Hein, and M. Valkama, “Radar scheme with raised reflector for NLOS vehicle detection,” *IEEE Transactions on Intelligent Transportation Systems*, 2021.
 - [21] A. Aubry, A. De Maio, and M. Rosamilia, “RIS-aided radar sensing in N-LOS environment,” in *IEEE International Workshop on Metrology for AeroSpace*, 2021, pp. 277–282.
 - [22] S. Buzzi, E. Grossi, M. Lops, and L. Venturino, “Foundations of MIMO radar detection aided by reconfigurable intelligent surfaces,” *IEEE Transactions on Signal Processing*, vol. 70, pp. 1749–1763, 2022.
 - [23] H. Zhang, H. Zhang, B. Di, K. Bian, Z. Han, and L. Song, “MetaRadar: Multi-target detection for reconfigurable intelligent surface aided radar systems,” *IEEE Transactions on Wireless Communications*, 2022, in press.
 - [24] K. V. Mishra, A. Chattopadhyay, S. S. Acharjee, and A. P. Petropulu, “OptM3Sec: Optimizing multicast IRS-aided multi-antenna DFRC secrecy channel with multiple eavesdroppers,” in *IEEE International Conference on Acoustics, Speech and Signal Processing*, 2022, in press.
 - [25] A. M. Elbir, K. V. Mishra, M. Shankar, and S. Chatzinotas, “The rise of intelligent reflecting surfaces in integrated sensing and communications paradigms,” *arXiv preprint arXiv:2204.07265*, 2022.
 - [26] T. Wei, L. Wu, K. V. Mishra, and M. R. B. Shankar, “Multiple IRS-assisted wideband dual-function radar-communication,” in *IEEE International Symposium on Joint Communications & Sensing*, 2022, pp. 1–5.
 - [27] M. I. Skolnik, *Radar handbook*, 3rd ed. McGraw-Hill, 2008.
 - [28] A. M. Elbir, K. V. Mishra, and Y. C. Eldar, “Cognitive radar antenna selection via deep learning,” *IET Radar, Sonar & Navigation*, vol. 13, no. 6, pp. 871–880, 2019.
 - [29] M. F. Ahmed, K. P. Rajput, N. K. Venkatesh, K. V. Mishra, and A. K. Jagannatham, “Joint transmit and reflective beamformer design for secure estimation in IRS-aided WSNs,” *IEEE Signal Processing Letters*, vol. 29, pp. 692–696, 2022.
 - [30] F. Gini, A. De Maio, and L. Patton, *Waveform design and diversity for advanced radar systems*. IET Press, 2012.
 - [31] A. Aubry, A. De Maio, M. Piezzo, A. Farina, and M. Wicks, “Cognitive design of the receive filter and transmitted phase code in reverberating environment,” *IET Radar, Sonar & Navigation*, vol. 6, no. 9, pp. 822–833, 2012.
 - [32] B. Zheng, C. You, W. Mei, and R. Zhang, “A survey on channel estimation and practical passive beamforming design for intelligent reflecting surface aided wireless communications,” *IEEE Communications Surveys & Tutorials*, 2022.
 - [33] W. Tang, X. Chen, M. Z. Chen, J. Y. Dai, Y. Han, S. Jin, Q. Cheng, G. Y. Li, and T. J. Cui, “On channel reciprocity in reconfigurable intelligent surface assisted wireless networks,” *IEEE Wireless Communications*, vol. 28, no. 6, pp. 94–101, 2021.
 - [34] Z. Esmaeilbeig, S. Khobahi, and M. Soltanalian, “Deep-RLS: A model-inspired deep learning approach to nonlinear PCA,” *arXiv preprint arXiv:2011.07458*, 2020.
 - [35] A. Eamaz, F. Yeganegi, and M. Soltanalian, “Modified arcsine law for one-bit sampled stationary signals with time-varying thresholds,” in *ICASSP 2021-2021 IEEE International Conference on Acoustics, Speech and Signal Processing (ICASSP)*. IEEE, 2021, pp. 5459–5463.
 - [36] S. M. Kay, *Fundamentals of statistical signal processing: Estimation theory*. Pearson Education, 1993, vol. 1.
 - [37] W. Lu, B. Deng, Q. Fang, X. Wen, and S. Peng, “Intelligent reflecting surface-enhanced target detection in MIMO radar,” *IEEE Sensors Letters*, vol. 5, no. 2, pp. 1–4, 2021.
 - [38] P. Z. Peebles, *Radar principles*. John Wiley & Sons, 2007.
 - [39] H. L. Van Trees, *Optimum array processing: Part IV of detection, estimation, and modulation theory*. John Wiley & Sons, 2004.
 - [40] P. Stoica and R. L. Moses, *Spectral analysis of signals*. Prentice Hall, 2005.
 - [41] M. Soltanalian and P. Stoica, “Designing unimodular codes via quadratic optimization,” *IEEE Transactions on Signal Processing*, vol. 62, no. 5, pp. 1221–1234, 2014.
 - [42] A. Ameri and M. Soltanalian, “One-bit radar processing for moving target detection,” in *IEEE Radar Conference*, 2019, pp. 1–6.
 - [43] E. Tohidi, M. Coutino, S. P. Chepuri, H. Behroozi, M. M. Nayebi, and G. Leus, “Sparse antenna and pulse placement for colocated mimo radar,” *IEEE Transactions on Signal Processing*, vol. 67, no. 3, pp. 579–593, 2018.